

Proton impact ionization and a fast calculation method

Xiaohua Fang,¹ Dirk Lummerzheim,² and Charles H. Jackman³

Received 21 April 2013; revised 26 July 2013; accepted 29 July 2013; published 22 August 2013.

[1] We present a coupled Monte Carlo and multistream model simulating primary ionization and secondary electron ionization, respectively, from energetic proton precipitation in the Earth's upper atmosphere. Good agreement is obtained with previous model results. It is found that while secondary electrons make a negligible contribution to ionization from low-energy (≤ 10 keV) auroral proton precipitation, their importance increases with increasing incident proton energy, confirming earlier findings. It becomes significant or even comparable to primary ionization from protons and generated hydrogen atoms in charge-changing collisions. Our calculations of the mean energy loss per ion pair production show a nearly monotonic increase with incident proton energy, ranging from about 22 eV to 33 eV when incident energy increases from 100 eV to 1 MeV. To facilitate a fast calculation in large-scale computations, we develop a parameterization for total (primary plus secondary) ionization from monoenergetic proton precipitation. This is obtained by fitting to a large set of numerical results from the coupled model. The quick method applies to a wide energy range of 100 eV to 1 MeV for incident monoenergetic protons, and its validity has been extensively tested under a variety of background atmospheric conditions. Our new parameterization can be used to rapidly calculate the ionization altitude profile from precipitating protons with any spectral distributions without any significant compromise in accuracy. By considering branching ratios of ionized atmospheric species, the fast calculation method is thus useful for self-consistently including proton impact effects in large community models.

Citation: Fang, X., D. Lummerzheim, and C. H. Jackman (2013), Proton impact ionization and a fast calculation method, *J. Geophys. Res. Space Physics*, 118, 5369–5378, doi:10.1002/jgra.50484.

1. Introduction

[2] Although in statistics and from a global perspective, a majority of precipitating particle energies into the Earth's upper atmosphere are carried by electrons [Hardy *et al.*, 1989; Emery *et al.*, 2008; Guo *et al.*, 2011], ion (specifically proton) precipitation can account for a significant fraction of the ionospheric conductance [Galand and Richmond, 2001; Galand *et al.*, 2001; Fang *et al.*, 2007a]. This fraction increases significantly in the equatorward portion of the duskside auroral oval [Hardy *et al.*, 1989]. In addition, studies show that proton precipitation can significantly affect ion convection and thermospheric composition and neutral winds [Galand *et al.*, 2001; Fang *et al.*, 2007b]. It is thus important to include the effects of precipitating protons, in addition to electrons, in understanding ionospheric

and thermospheric properties and disturbances particularly during space weather events.

[3] Since most of the incident proton energy is lost to the upper atmosphere through ionizing processes [Basu *et al.*, 1987; Fang *et al.*, 2004], understanding particle impact ionization is a key component to assessing the role of proton precipitation in the coupling between the magnetosphere and the thermosphere/ionosphere. It is worth noting that the term “ionization” here and throughout this paper refers to ion production in ionizing collisions (including direct ionization and charge exchange collisions) between primary/secondary energetic particles and ambient neutrals. A number of models have been developed over decades to calculate the variation of proton impact ionization along particle penetration. These models can be generally grouped into three categories: range calculation (in the continuous slowing-down approximation) [e.g., Jackman *et al.*, 1980; Rees, 1982], linear transport theoretical treatment [e.g., Jasperse and Basu, 1982; Basu *et al.*, 1987], and Monte Carlo method [e.g., Kozelov, 1993; Fang *et al.*, 2004]. As secondary electrons are generated and undergo distinct different collisional processes with ambient neutrals, a complete description of proton impact geoeffectiveness requires the coupling with electron transport calculations [e.g., Strickland *et al.*, 1993; Solomon, 2001]. For an extensive list of references on proton precipitation studies, see also the review by Basu *et al.* [2001] and Fang *et al.* [2004]. Regardless of the degree

¹Laboratory for Atmospheric and Space Physics, University of Colorado Boulder, Boulder, Colorado, USA.

²Geophysical Institute, University of Alaska Fairbanks, Fairbanks, Alaska, USA.

³NASA Goddard Space Flight Center, Greenbelt, Maryland, USA.

Corresponding author: X. Fang, Laboratory for Atmospheric and Space Physics, University of Colorado Boulder, 3665 Discovey Dr., Boulder, CO 80303, USA. (xiaohua.fang@lasp.colorado.edu)

of approximations and accuracy, a common problem with these models is computational intensity and complexity, making it practically infeasible to self-consistently add proton impact effects into large-scale calculations in modern global models.

[4] Recent rapid development of high performance and parallel computing has accelerated the trend of studying near-Earth space as a system while allowing for various physical processes on a global scale. However, modern global models are still forced by limitations on computer resources to parameterize as many processes as possible. As the details of local collisional effects associated with proton precipitation are reasonably understood, it is a natural need to have a fast and accurate parameterization for proton impact effects to be included and examined in a system context.

[5] *Rees* [1982] outlined a simple method to perform a fast estimate of the ionization altitude profile from precipitating monoenergetic 200 eV to 60 keV protons. It is based on simplistic range calculation and assumes a constant mean energy loss per ion pair production of $W = 36$ eV. As will be shown later, the mean energy loss actually is energy dependent. Taking the *Rees* [1982] method as a starting framework, *Galand et al.* [1999] improved the method by using a 1-D multistream transport model and developed a parameterization of ion and electron production rates for incident Maxwellian proton distributions with a characteristic energy between 1 and 20 keV. A Maxwellian distribution is described by

$$\phi(E) = \frac{Q_0}{2E_0^3} E \exp\left(-\frac{E}{E_0}\right), \quad (1)$$

where ϕ is the differential hemispherical number flux of incident protons ($\text{keV}^{-1} \text{cm}^{-2} \text{s}^{-1}$), Q_0 is the total incident energy flux ($\text{keV cm}^{-2} \text{s}^{-1}$), and E_0 is the characteristic energy in keV. The average energy is $\langle E \rangle = 2E_0$. It should be pointed out that the complexity of the problem makes deriving parameterization of ionization rates for individual atmospheric species a challenging task. The common approach in these parameterizations is to derive the total ionization rate and then break it down by applying cross section-based branching ratios [see *Galand et al.*, 1999].

[6] There are several limitations of the *Galand et al.* [1999] parameterization in its application. First, the derivation of the parameterization itself does not include the ionization from secondary electrons, which is important when incident proton energies are high. It was suggested that this secondary ionization could be estimated using a separate study of *Lilensten and Galand* [1998], which approximated the secondary ionization addition with an altitude-independent fraction of $0.006 \times E_0$. Note that the *Lilensten and Galand* [1998] approximation is a very rough estimate based on a limited number of energy cases, having a significant deviation even from their own model results at $E_0 = 1$ keV. Second, the *Galand et al.* [1999] parameterization is applicable to only auroral protons in a Maxwellian distribution. While the Maxwellian spectral approximation sometimes proves convenient [e.g., *Sharber*, 1981], it might also introduce significant errors in describing precipitation conditions and thus the concomitant geoeffectiveness. For instance, the high-energy tail in particle distributions [e.g., *Lyons and Evans*, 1984] cannot be represented by the

Maxwellian approximation, and significant errors may arise [*Fang et al.*, 2010; *Lanchester et al.*, 2011].

[7] A general solution to complex precipitation conditions is to develop a parameterization for calculating monoenergetic proton impact ionization. Any incident spectrum can be divided into a number of energy bins that are sufficiently fine so that particles within them can be regarded to have a single energy value. By this means, the monoenergetic parameterization can be applied and the final result can be obtained by integrating the ionization over the bins. This is the strategy we will take in this study. The paper is organized as follows. In section 2, we couple a Monte Carlo proton/hydrogen transport model with a multistream electron transport model to include secondary electron effects in ionization calculations. In section 3, a new parameterization is derived based on the total ionization results from the sophisticated coupled model, and its validity is systematically examined. The paper concludes in section 4.

2. Coupled Monte Carlo and Multistream Model

2.1. Model Description

[8] The 3-D Monte Carlo model of *Fang et al.* [2004, 2005, 2007a, 2007b] is used to calculate primary ionization from precipitating protons. The detail of the model has been documented by *Fang et al.* [2004] and is not repeated. Rather, we provide brief model descriptions here. By monitoring the random walk of millions of test protons starting from 950 km altitude as well as atomic hydrogens generated through charge exchange collisions, we simulate the inelastic collisions (ionization, charge exchange/electron stripping, and excitation) and elastic collisions between energetic projectiles (H^+/H) and neutral atmospheric targets (O , N_2 , and O_2). A forward scattering approximation is applied to inelastic collisions following *McNeal and Birely* [1973], and angular scattering is allowed for elastic collisions following *Kallio and Barabash* [2001]. Along the path of particles, protons and hydrogens are coupled with their charge state shifting back and forth due to charge exchange (for H^+) and electron stripping (for H) collisions. The primary ionization rate is obtained by counting the production rate of new ions of the atmospheric origin in all these processes. By this means, the ionization rate result is naturally obtained in the model. There is no need (and it is not accurate) to use an approximate mean energy loss to divide the energy deposition rate, as done by *Rees* [1982]. We calculate the production of secondary electrons as a function of altitude, energy, and angle, following *Solomon* [2001].

[9] In our Monte Carlo modeling of proton/hydrogen transport, the differential cross sections for inelastic and elastic collisions are from *Basu et al.* [1987] and *Kallio and Barabash* [2001], respectively. However, these cross sections are partly incomplete, particularly at the high-energy end around 1 MeV. Specifically, there is no energy coverage above 300 keV for charge exchange collisions and hydrogen atom-induced ionization collisions (except those between H and O). A linear extrapolation on a log-log scale has been performed to fill in the gaps of the cross sections. Although uncertainties exist in model results due to insufficient cross-section data availability, the overall agreement among existing proton/hydrogen transport models (even though different methodologies were used) is reasonably

good [e.g., *Decker et al.*, 1996; *Solomon*, 2001]. The agreement between theoretical results and observational data [e.g., *Basu et al.*, 1987] indicates that the physical picture of the collisional processes during energetic proton precipitation is basically correct, while quantitative accuracy is limited mainly by cross-section data. A quantitative evaluation of how uncertainties propagate from cross-section data to model outputs, which requires not only a compilation of lab measurements but also extensive numerical experiments, is beyond the scope of this study. Rather, the focus of this work is on consistent integration of relevant models for a complete picture of proton impact effects and on the development of a fast calculation method suitable for large-scale computations.

[10] It should be pointed out that the transverse proton-hydrogen beam spreading effect, which is due to charge-changing collisions [e.g., *Jasperse and Basu*, 1982; *Kozelov*, 1993; *Fang et al.*, 2004, 2005, 2007a, 2007b], is not included in this study. Although such an effect may be significant particularly along the edge of proton arcs, we neglect it as a first-order approximation. The inclusion of the beam spreading effect would greatly increase the complexity of the problem but add only a second-order correction. Without taking this effect into account, the results presented in this paper are valid when the incident proton arc at the top is large and quasi-uniform in terms of the energy distribution [cf. *Fang et al.*, 2005]. Note that the old parameterizations of *Rees* [1982] and *Galand et al.* [1999], as well as the models on which these parameterizations were based, omitted the beam spreading effect due to their 1-D nature. Although a correction factor has been introduced by 1-D models [e.g., *Jasperse and Basu*, 1982] to approximate the attenuation at beam centers, *Fang et al.* [2005] found that the altitude-independent characteristic and the neglect of the difference of spreading between particle fluxes and ionization rates made the simplistic correction not much helpful. Taking the complex beam spreading into account in parameterization will be the goal of a future study.

[11] The Monte Carlo model-calculated secondary electrons provide a source term to the multistream model of *Lummerzheim et al.* [1989] and *Lummerzheim and Lilensten* [1994] for further ionization calculation. The differential electron flux distribution is calculated by solving steady state Boltzmann transport equations with collisional processes (and associated energy loss and angular scattering) considered. The ionization rate then can be calculated by integrating the product of the flux, neutral densities, and relevant cross sections with respect to energy and pitch angle. Note that although the full spectrum of secondary electron production is available from the Monte Carlo model, we simplify the problem by assuming an isotropic approximation before applying it to the multistream model. This is a reasonable assumption without compromising the accuracy of the model, given the fact that subsequent scattering quickly removes any anisotropy in the initial angular distribution [*Basu et al.*, 1993; *Solomon*, 2001]. *Lummerzheim et al.*, [1989] made experiments with nonisotropic secondaries and found no significant changes in their results.

2.2. Model Results

[12] By combining the Monte Carlo proton/hydrogen model and the multistream electron model, we obtain a

complete picture of the interaction of incident protons (and generated hydrogen atoms and secondary electrons) with the Earth's upper atmosphere and the resulting ionization. All the results shown in this study are for an incident energy flux of $1 \text{ erg cm}^{-2} \text{ s}^{-1}$ (or $6.24 \times 10^8 \text{ keV cm}^{-2} \text{ s}^{-1}$), regardless of energy spectra. The background magnetic field is assumed to be vertical to the ground. The effect of the dip angle of the magnetic field line, which is relatively insignificant, can be estimated using the results from *Fang et al.* [2005]. The atmosphere is specified using the Mass Spectrometer Incoherent Scatter (MSIS-90) model [*Hedin*, 1991]. Unless otherwise noted, the MSIS-90 atmosphere is specified for 70° latitude at midnight in spring.

[13] An example result from the coupled Monte Carlo and multistream model (henceforth "MCMS") is shown in Figure 1. There is a very good agreement between our MCMS results and *Solomon* [2001] (in which a coupled 1-D Monte Carlo and two-stream model was used), for both primary ionization and secondary electron ionization. The comparison with the *Galand et al.* [1999] parameterization on primary ionization (magenta curves versus square symbols and blue dashed curves), however, shows a significant discrepancy: more than 25% in the peak values. Such a difference may be in part attributed to the error of the old parameterization in fitting to their transport model results, which can be as high as $\sim 20\%$ [*Galand et al.*, 1999]. The remaining discrepancy may be due to the differences in model treatments and cross-section selections [cf., *Decker et al.*, 1996]. Despite the overall agreement, *Solomon* [2001] found that his Monte Carlo model produced less primary ionization but more secondary ionization than prevailing linear transport models due to different assumptions and approximations in secondary electron production and energy allocation. An important observation from Figure 1 is that the ratio of secondary electron ionization to primary ionization increases with increasing incident energy; that is, its importance changes from negligible at $E_0 = 4 \text{ keV}$ to nearly comparable at $E_0 = 100 \text{ keV}$. We will revisit this topic later with more quantitative analyses.

[14] Another validation of the MCMS model is presented in Figure 2, where we compare the total ionization rate with that from range calculation for precipitating protons with an energy of $E_{\text{mono}} = 1 \text{ MeV}$. Here we use the subscript "mono" to indicate that incident protons are monoenergetic. The range calculation technique simply scales laboratory measurements to the atmosphere and assumes a continuous energy loss along the particle penetration depth. The (total) ionization rate is obtained by dividing the energy absorption rate by an averaged energy loss of 35 eV [*Jackman et al.*, 1980]. Because angular redistribution (which however becomes important at low energies [*Kallio and Barabash*, 2001; *Fang et al.*, 2004]) is not considered in such a technique, range calculation is regarded more appropriate for incident high-energy particles. Therefore, this simple technique is not invoked anymore for auroral particles, but is commonly accepted for solar energetic protons whose energies are of the order of MeV and higher. In our application of this approach for the comparison in Figure 2, we follow *Jackman et al.* [1980] but replace the simplified range-energy relationship with more direct and accurate stopping-power data published by National Institute of Standards

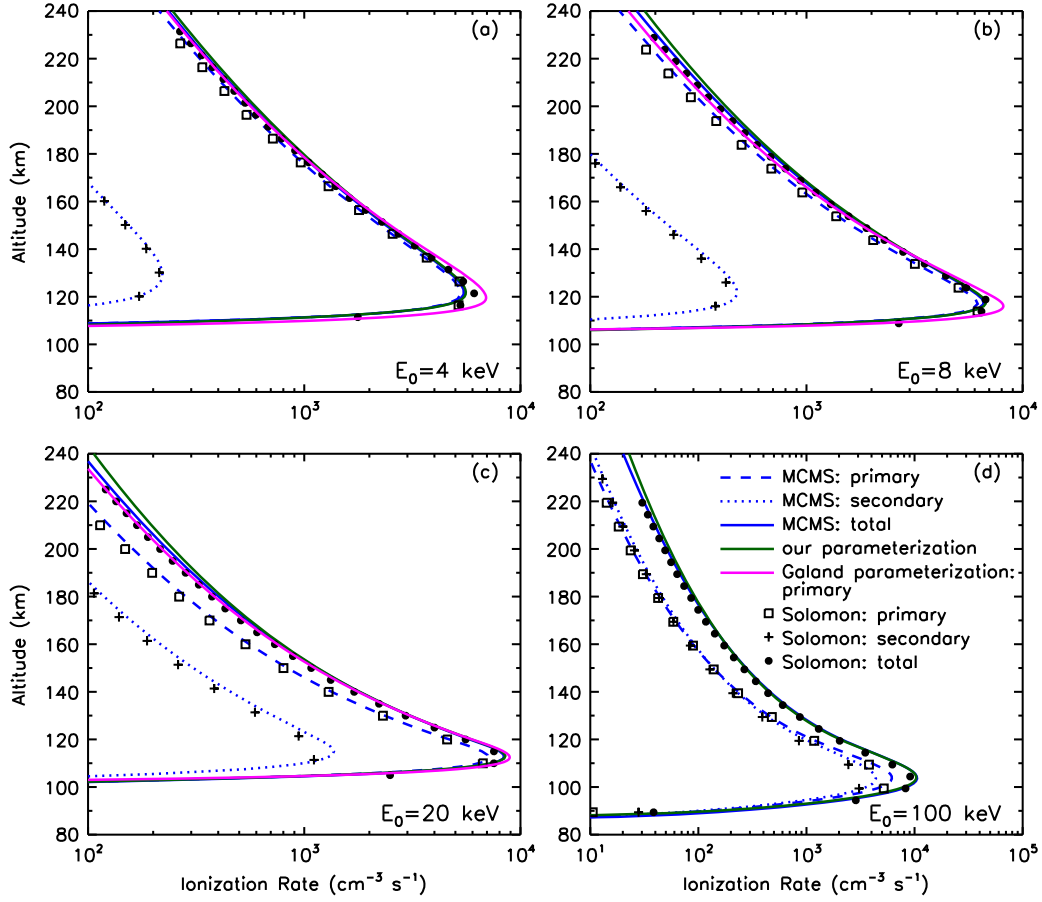


Figure 1. Comparison of ionization rates using different methods: our coupled Monte Carlo and multistream model (in blue; dashed for primary ionization, dotted for secondary electron ionization, solid for total ionization), our new parameterization (in green, total ionization), *Galand et al.* [1999] parameterization (in magenta, primary ionization), and *Solomon* [2001] (square for primary, plus for secondary, dot for total). The panels show the results when incident protons have a Maxwellian distribution with a characteristic energy: (a) $E_0 = 4$ keV, (b) $E_0 = 8$ keV, (c) $E_0 = 20$ keV, and (d) $E_0 = 100$ keV. Note that in Figure 1d, there is no corresponding result from the *Galand et al.* [1999] parameterization as the energy is outside of its applicable limit. The MSIS-90 atmosphere is specified using $F_{10.7} = 289$, $\langle F_{10.7} \rangle = 209$, $A_p = 15$, latitude = 65° , longitude = -160° , and UT = 0. The background magnetic field line is vertical to the ground.

and Technology [Berger *et al.*, 2011]. Figure 2 shows a good agreement between the MCMS model and range calculation despite a slight difference ($\sim 11\%$ at peak altitudes). Note that the difference between the model results at high altitudes is negligible where the ionization rate is more than two orders of magnitude lower than the peak intensity. The discrepancy at low altitudes can be explained by two reasons. First, a constant mean energy loss of 35 eV is used by the range calculation approach, which, as will be shown below, is overestimated at $E_{\text{mono}} = 1$ MeV and thus leads to an underestimation of the ionization. Second, angular scattering becomes important at low energies when particles penetrate deep into the atmosphere and lose most of the incident energy there. This scattering effect partly explains why the sophisticated MCMS model predicts a slightly shorter penetration depth and a higher peak ionization rate.

[15] Figure 3 presents the MCMS model-calculated mean energy loss per ion pair production as a function of incident particle energy. The mean energy loss per ion pair

produced W is defined as the total energy influx at the top divided by altitude-integrated ionization in the atmosphere [e.g., Strickland *et al.*, 1993]:

$$W = \frac{\int_0^\infty E\phi(E) dE}{\int_0^\infty q_{\text{tot}}(z) dz}, \quad (2)$$

where q_{tot} is the total ionization rate ($\text{cm}^{-3} \text{s}^{-1}$). W thus serves as a good proxy of the particle ionizing efficiency; that is, smaller W values indicate a higher level of the ionizing efficiency on average. Because of forward scattering in inelastic collisions, which are dominant over elastic collisions for high-energy projectiles [see Fang *et al.*, 2004], the energy outflux carried by backward scattered particles is insignificant.

[16] In order to check the sensitivity of the results to the background neutral density profile, we perform the calculations using 36 MSIS-90 model atmospheres by varying $F_{10.7}$ (50, 100, 150, 200, 250, and 300) and A_p (5, 25, 50, 100,

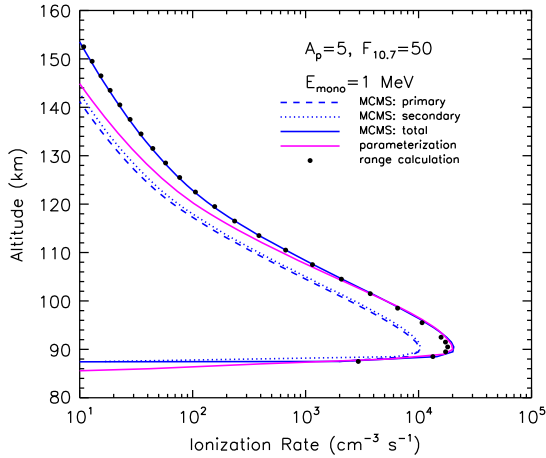


Figure 2. Comparison of ionization rates among the MCMS model (in blue; dashed for primary ionization, dotted for secondary electron ionization, solid for total ionization), the new parameterization (in magenta), and a range calculation approach (dots). The results are given for monoenergetic proton injection of $E_{\text{mono}} = 1$ MeV.

150, and 200) indices. As seen in Figure 3, the W value is essentially independent of the atmosphere. However, there is a general increasing trend of W with an increase in proton energy: from $W = 21.98$ eV at $E_{\text{mono}} = 100$ eV to $W = 32.76$ eV at $E_{\text{mono}} = 1$ MeV. That is, in general, lower-energy precipitating protons have a higher efficiency in ionizing the atmosphere. An exception to this general upward trend of W occurs at the low end of the energy range under consideration. The W value slightly drops with increasing E_{mono} until a minimum of 21.36 eV is reached at 260 eV. However, care must be taken because this $\sim 3\%$ difference in W between $E_{\text{mono}} = 100$ eV and 260 eV is much smaller than the uncertainties in collision cross-section data used in the numerical simulations. Figure 3 shows that the MCMS model-calculated mean energy loss for $E_{\text{mono}} \leq 1$ MeV is slightly smaller than 35 eV (with a percentage difference of 6%), which explains the discrepancy we have seen in Figure 2 with range calculation. Similarly, a note of caution on cross sections is needed in interpreting this difference. The lack of a full understanding of collision cross sections may also account for the slight variation of W at around $E_{\text{mono}} = 800$ keV in Figure 3. However, the reasonable agreement with range calculation as demonstrated in Figure 2, which is based on laboratory measured energy loss and is commonly accepted for very energetic particle precipitation, shows that such uncertainties are not problematic.

[17] We continue the mean energy loss discussion in Figure 4, where the W value is examined for precipitating protons in a Maxwellian distribution. An initial observation from Figure 4 is the large divergence of published model results. The maximum intermodel difference in W is as high as 16 eV at $E_0 = 1$ keV. The model divergence decreases with increasing energy, reaches a minimum of 3 eV at $E_0 = 10$ keV, and then slightly increases again. As noticed by *Galand et al.* [1999], the relatively high W values from *Strickland et al.* [1993] at low energies is mainly due to an inappropriately set low-energy cutoff in calculations. *Decker et al.* [1996] found that the high W values

from *Kozelov and Ivanov* [1994] could be explained by larger low-energy excitation cross sections in their calculations. In addition, after taking secondary electron ionization into account, the *Decker et al.* [1996] results would have been lowered. Therefore, if omitting the apparent deviation at low energies from *Strickland et al.* [1993] and *Kozelov and Ivanov* [1994], we can see that the models actually have a reasonably good agreement, with a < 3 eV inter-model difference (which, to a large degree, is due to different cross-section selections).

[18] We have seen in Figure 1 the contribution of secondary electrons to total ionization yield and the variation with incident proton energy. In Figure 5, a quantitative analysis is provided. It is seen in Figure 5a that secondary ionization is reasonably negligible for a typical proton aurora (for example, $E_{\text{mono}} \leq 10$ keV), consistent with previous studies [*Strickland et al.*, 1993; *Basu et al.*, 2001]. However, for precipitation consisting of more energetic ring current protons and solar energetic protons, secondary electrons contribute to the ionization at a significant or even comparable level, and thus must be included.

[19] It is of interest to notice that the secondary-to-primary ratio is smaller when we examine it for peak ionization in comparison with altitude-integrated ionization: varying from $\sim 24\%$ smaller at $E_{\text{mono}} = 1$ keV to $\sim 44\%$ smaller at $E_{\text{mono}} = 100$ keV. This can be roughly explained as follows. First, ionization falls off rapidly below the peak, and a bigger part of altitude-integrated ionization comes from the high-altitude region above the peak. This means that the average energy of particles (for both primary H^+/H and secondary e^-) in ionizing collisions is generally greater for altitude-integrated ionization than that for peak ionization. Second, as seen in Figure 3, protons with a lower energy have a smaller W value and thus a higher ionizing efficiency, which is understandable considering the increased efficiency of charge exchange-induced ionization at low energies (see *Basu et al.* [1987] for the comparison of collisional cross sections). In contrast, lower-energetic electrons have a lower ionizing efficiency [e.g., *Fang et al.*, 2008; *Simon Wedlund et al.*, 2011]. Combining these two reasons

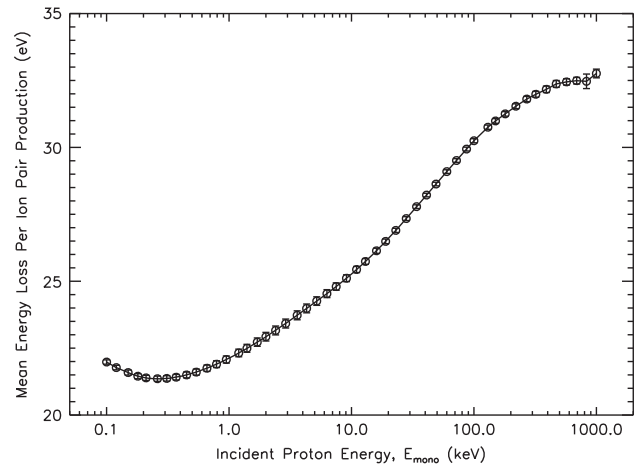


Figure 3. Mean energy loss per ion pair production for monoenergetic proton precipitation. Open circles indicate mean values when the background atmosphere varies (see text), and error bars represent one standard deviation.

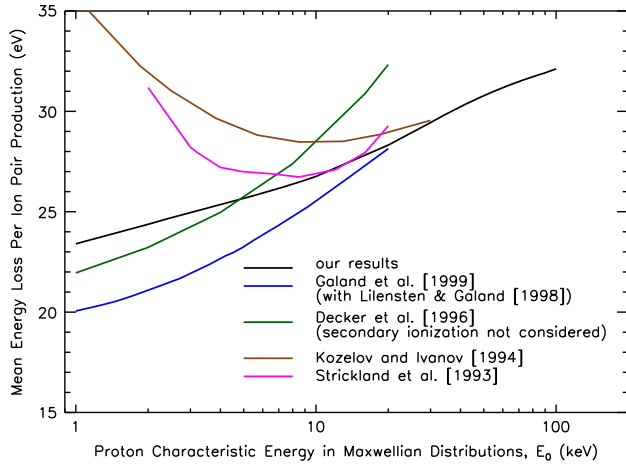


Figure 4. Mean energy loss per ion pair production for Maxwellian proton precipitation. All of the results for comparison here have considered secondary electron ionization, except for *Decker et al.* [1996]. Note that the *Galand et al.*, [1999] parameterization itself did not include secondary electron ionization. Their results shown here were obtained by applying a simplistic estimate of *Lilensten and Galand* [1998] to approximate the secondary effect.

offers a coherent view of how the secondary-to-primary ratio differs when comparing altitude-integrated ionization and peak ionization. Similarly, the different dependence of the ionizing efficiency on energy between protons and electrons can help understand why secondary electron ionization peaks at a slightly higher location than primary ionization, as seen in Figure 5b. Finally, Figure 5c shows that higher-energetic precipitating protons lead to a deeper penetration in general. Because less energetic incident particles stop at a higher altitude where the atmosphere is more sensitive to solar/geomagnetic activities, the peak ionization location is more variable with the background atmospheric conditions at lower energies, as shown in Figure 5c.

3. Parameterization of Monoenergetic Proton Impact Ionization

3.1. Parameterization Scheme

[20] The coupled Monte Carlo and multistream model provides a rigorous approach for calculating primary and secondary ionization rates from proton precipitation. However, it is not suitable for a direct practical application due to its high requirement on computational effort. In particular, the Monte Carlo technique costs a large amount of CPU time by tracing transport and collisions of a large number of test particles, and thus cannot satisfy the need of fast calculation in large-scale simulations. A quick calculation method (or parameterization) based on the results from the sophisticated coupled model represents an optimal solution: it avoids an unreasonable amount of computing effort while keeping the numerical results as accurate as possible.

[21] To derive the parameterization of proton impact total ionization (primary plus secondary), we follow the robust yet flexible algorithm that was recently developed for electron precipitation by *Fang et al.* [2008, 2010]. There are

basically three steps in this scheme. First, the resulting ionization altitude profiles under various atmospheric conditions over a wide precipitating energy range are calculated using the MCMS model. Second, these physical results are reorganized using two normalized quantities: normalized energy dissipation rates (to replace ionization rates) and normalized atmospheric column masses (to replace altitude). The purpose of this reorganization is to ensure that the vertical variation of the results follows the same form for any given precipitating energy, no matter what background atmospheres are applied. Third, a 2-D curve fitting is then performed to derive empirical formulae. Below, we will describe these steps in more detail.

[22] In the first step, the MCMS model has been run for 50 precipitating proton monoenergies, which are uniformly scattered on a logarithmic scale from 100 eV to 1 MeV. For each of the incident energies, the background atmosphere varies by changing the $F_{10.7}$ and A_p indices in the MSIS-90 model. $F_{10.7}$ varies from 50 to 300 by a step of 50 to reflect different solar activities, and A_p varies among 5, 25, 50, 100, 150, and 200 to reflect various geomagnetic activities. That is, extensive calculations have been made for a total of 1800 cases: 50 energies by 36 atmospheres.

[23] In the next step, we define two normalized quantities for monoenergetic proton precipitation. One is normalized

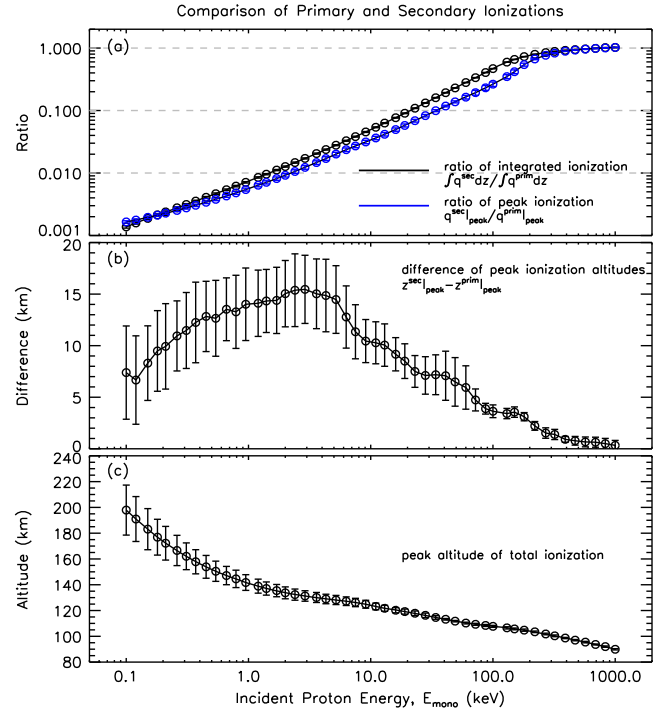


Figure 5. Shown here are (a) ratios of altitude-integrated secondary electron ionization rates to primary ionization (black) and ratios of peak secondary ionization rates to peak primary ionization (blue), (b) difference of peak ionization altitudes between secondary and primary ionization, and (c) peak altitudes of total ionization. The results are given for monoenergetic proton precipitation. Open circles and error bars have the same meaning as in Figure 3.

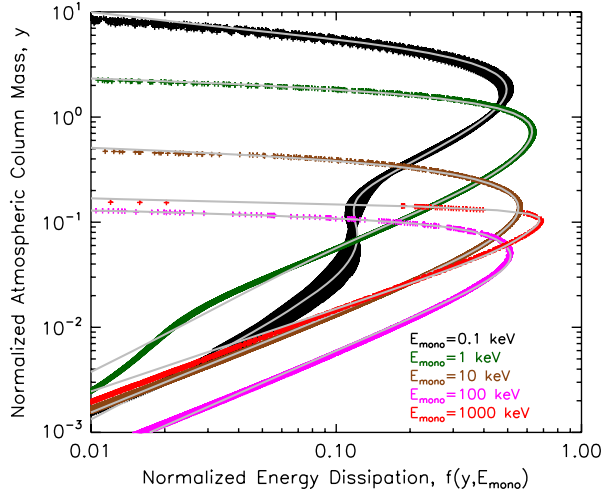


Figure 6. Results in terms of normalized energy dissipation and normalized atmospheric column mass for five representative incident proton energies: $E_{\text{mono}} = 0.1, 1, 10, 100,$ and 1000 keV. The plus symbols show the results obtained from the MCMS model, and the gray curves are from the new parameterization.

energy dissipation (f):

$$f = q_{\text{tot}}(z) \left(\frac{Q_{\text{mono}}}{\Delta\epsilon} \frac{1}{H(z)} \right), \quad (3)$$

where q_{tot} is the sum of primary ionization and secondary electron ionization ($\text{cm}^{-3} \text{s}^{-1}$), Q_{mono} is the incident H^+ energy flux ($\text{keV cm}^{-2} \text{s}^{-1}$), $\Delta\epsilon$ is a constant of 0.035 keV, and $H(z)$ is the atmospheric scale height (cm) given by

$$H(z) = \frac{kT(z)}{m(z)g(z)}, \quad (4)$$

where k is the Boltzmann constant, T is the atmospheric temperature, m is the average molecular weight, and g is the acceleration of gravity. It is worth noting that a constant “mean energy loss” ($\Delta\epsilon$) is applied here solely for empirically deriving a parameterization. In our calculations with the coupled model, to which we fit the parameterization, the actual mean energy loss results (W) as shown in Figure 3 are the model output, not input. Thus, there is no conflict between the energy-dependent W obtained from the coupled model and the constant $\Delta\epsilon$ empirically used in the parameterization.

[24] The other quantity introduced for the parameterization is normalized atmospheric column mass (y), which is defined as

$$y = \frac{7.5}{E_{\text{mono}}} \left(\frac{\rho(z)H(z)}{10^{-4}} \right)^{0.9}, \quad (5)$$

where E_{mono} is incident proton energy (keV), and ρ is mass density of the atmosphere (g cm^{-3}).

[25] Figure 6 shows an example result of the MCMS model after data reorganization. The strong sensitivity with respect to the background atmospheric profile, which is particularly prominent for low-energy proton precipitation and has been clearly illustrated in Figure 5, is removed. This is exactly what we need before a data fit is performed. The successful removal of the atmospheric sensitivity also justifies

the definitions of the two normalized quantities. The f - y relationship as shown in Figure 6 describes how much energy is lost locally when the projectile passes through a given mass of the atmosphere, which is also the basic idea of range calculation. It should be pointed out that although our parameterization is based on the physics-based MCMS model and the normalized quantities have clear physical meaning, the f and y definitions in equations (3) and (5) are empirically determined.

[26] In the final step of parameterization, we will use the reorganized model results to construct the dependence of f on y and E_{mono} . We assume a nonlinear form for their relationship, given by

$$f(y, E_{\text{mono}}) = C_1 y^{C_2} \exp(-C_3 y^{C_4}) + C_5 y^{C_6} \exp(-C_7 y^{C_8}) + C_9 y^{C_{10}} \exp(-C_{11} y^{C_{12}}). \quad (6)$$

Each parameter C_i ($i = 1, \dots, 12$) is energy dependent and is given by

$$C_i(E_{\text{mono}}) = \exp \left(\sum_{j=0}^3 P_{ij} (\ln(E_{\text{mono}}))^j \right). \quad (7)$$

That is, a third-order polynomial is assumed on a logarithmic scale ($\ln(C_i)$ versus $\ln(E_{\text{mono}})$), where \ln denotes the natural logarithm. Finally, the problem amounts to figuring out the values of 48 P_{ij} coefficients ($i = 1, \dots, 12; j = 0, \dots, 3$) in the above $f(y, E_{\text{mono}})$ function. To solve this problem, a least chi-square technique is used to fit the 2-D dependence to the data. The best fit results are presented in Table 1.

3.2. Verification

[27] The f - y relationship obtained from the new parameterization is examined in Figure 6 for five representative incident energies spanning 4 orders of magnitude. The results are in excellent agreement, in general, with those computed directly from the MCMS model. It is worth noting that the deviation at the two ends of the profiles does not cause any appreciable errors on the altitude-integrated ionization rates, since it takes place at weak ionization regions far from the peak altitudes.

[28] The comparison continues in Figures 2 and 7, where the ionization rate altitude profiles from the MCMS model and the new parameterization are compared with each other in different atmospheres. It is seen that the ionization distributions are well reproduced by the new parameterization,

Table 1. Parameterization Coefficients P_{ij} in Equation (7)

P_{ij}	$j = 0$	$j = 1$	$j = 2$	$j = 3$
$i = 1$	2.55050E+0	2.69476E-1	-2.58425E-1	4.43190E-2
$i = 2$	6.39287E-1	-1.85817E-1	-3.15636E-2	1.01370E-2
$i = 3$	1.63996E+0	2.43580E-1	4.29873E-2	3.77803E-2
$i = 4$	-2.13479E-1	1.42464E-1	1.55840E-2	1.97407E-3
$i = 5$	-1.65764E-1	3.39654E-1	-9.87971E-3	4.02411E-3
$i = 6$	-3.59358E-2	2.50330E-2	-3.29365E-2	5.08057E-3
$i = 7$	-6.26528E-1	1.46865E+0	2.51853E-1	-4.57132E-2
$i = 8$	1.01384E+0	5.94301E-2	-3.27839E-2	3.42688E-3
$i = 9$	-1.29454E-6	-1.43623E-1	2.82583E-1	8.29809E-2
$i = 10$	-1.18622E-1	1.79191E-1	6.49171E-2	-3.99715E-3
$i = 11$	2.94890E+0	-5.75821E-1	2.48563E-2	8.31078E-2
$i = 12$	-1.89515E-1	3.53452E-2	7.77964E-2	-4.06034E-3

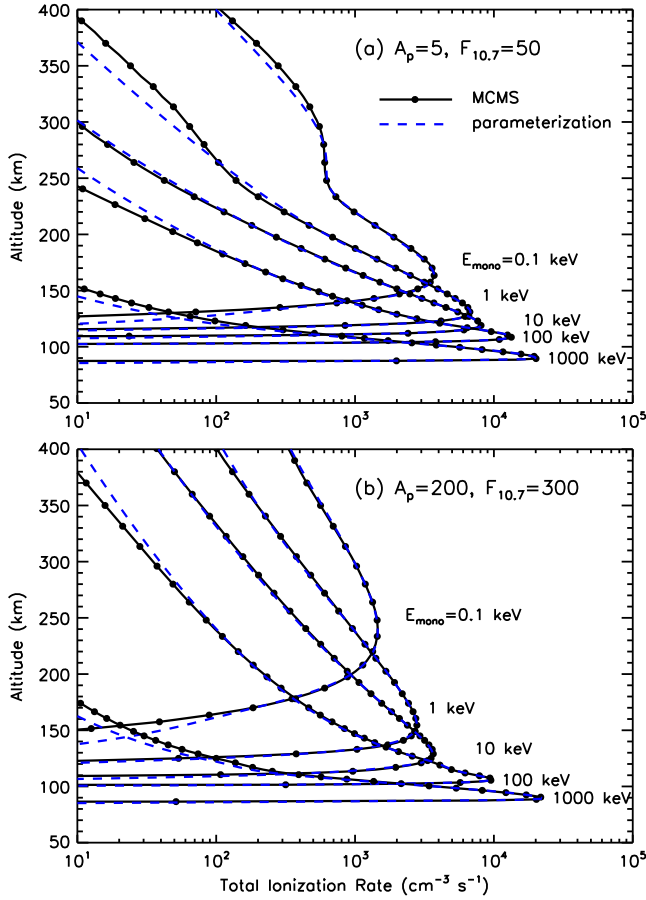


Figure 7. Total ionization rate altitude profiles from precipitating protons with an energy of $E_{\text{mono}} = 0.1, 1, 10, 100, 1000$ keV. Comparison is made between the results from the MCMS model (solid curves with dots) and the new parameterization (blue dashed). The two panels present the results in different MSIS-90 atmospheres specified using (a) $A_p=5, F_{10.7}=50$ and (b) $A_p=200, F_{10.7}=300$, respectively.

regardless of how distinct the background atmospheres are. Like what has been seen in Figure 6, noticeable deviation only occurs at low and high altitudes, where ionization is at least one and usually two or more orders of magnitude lower than peak intensities. That is, the corresponding errors are not considered significant.

[29] In addition to the comparison in the example cases, a systematic error analysis is conducted to test the validity of the new parameterization for more incident energies and under more atmospheric conditions. The test is performed for 50 incident proton energies ranging from 100 eV to 1 MeV, and under 36 atmospheric conditions that are associated with low to high solar/geomagnetic activities (same as those used for deriving the parameterization in section 3.1). Figure 8 presents the error analysis results on three aspects: altitude-integrated ionization in the atmosphere, peak ionization, and peak altitude. It is seen that a high level of agreement is achieved in all of these: less than $\pm 3\%$ errors in integrated ionization, less than $\pm 4\%$ in peak ionization rates, and less than ± 2 km in peak ionization altitudes (except for low incident energies of $E_{\text{mono}} < 200$ eV where the deviation may be up to 4 km). For lower-energy proton precipita-

tion, the error bars are larger because ionizing collisions occur at higher altitudes (see Figure 5) where the atmosphere varies more significantly with solar/geomagnetic activity level [Hedin, 1991].

3.3. Application

[30] With the new parameterization, we have a fast estimate of proton impact ionization rates along the particle penetration depth. While computational effort is considerably saved by applying the parameterization, accuracy is not compromised and is comparable to that of the sophisticated MCMS model. In order to apply the rapid method for precipitating protons with arbitrary energy spectra $\phi(E)$, the following steps are taken.

[31] First, the incident spectrum is uniformly divided into a sufficiently large number of energy bins on a logarithmic scale (say N), within which particles can be regarded monoenergetic. Within each bin k ($k = 1, \dots, N$), the energy influx is reasonably approximated to be $E_k \phi(E_k) \Delta E_k$. Second, the normalized column mass at a given altitude z for incident E_k , say $y(z, E_k)$, is calculated following equations (4) and (5). Third, the normalized energy dissipation $f(y, E_k)$ is obtained using equations (6) and (7) and Table 1. Finally, the total ionization rate at z is obtained

$$q_{\text{tot}}(z) = \frac{1}{\Delta \epsilon H(z)} \sum_{k=1}^N E_k \phi(E_k) \Delta E_k f(y, E_k). \quad (8)$$

[32] An example of applying the new parameterization to Maxwellian proton distributions is shown in Figure 1, where excellent agreement with the MCMS model is demonstrated.

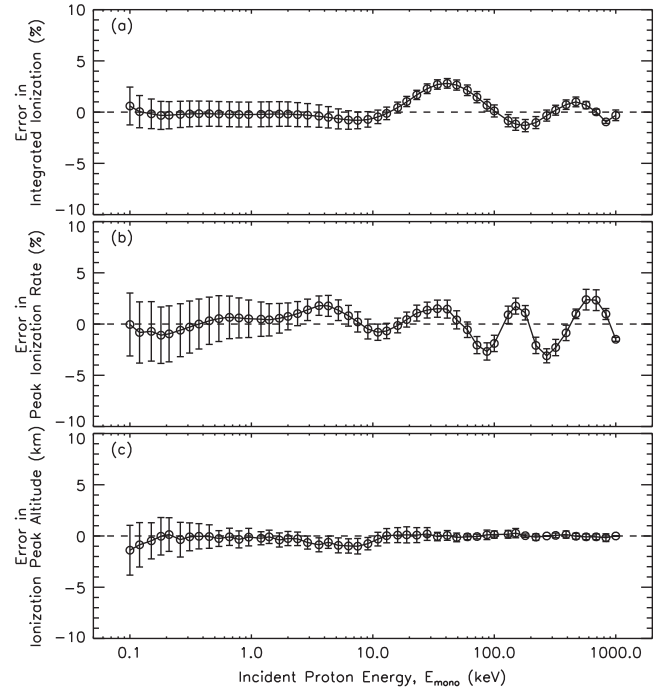


Figure 8. Comparison of (a) altitude-integrated total ionization, (b) peak ionization, and (c) peak altitudes between the new parameterization and the MCMS model. Open circles indicate the mean of the differences in a set of 36 MSIS-90 atmospheres. Error bars represent one standard deviation from the mean.

To better understand this agreement, we notice two challenges involved in the calculations. First, the background atmosphere in Figure 1 is specified using a different set of $F_{10.7}$ and A_p than the 36 atmospheres we used in parameterization derivation. Second, as illustrated in equation (8), ionization with altitude would have been erroneous if the contribution from each incident monoenergetic component was not correctly reproduced from our parameterization. The satisfactory comparison shown in Figure 1, together with Figure 8, indicates that our parameterization method is sufficiently robust to wide variations in precipitating energies and atmospheric conditions.

4. Discussion and Summary

[33] We have coupled a Monte Carlo proton/hydrogen transport model and a multistream electron transport model to calculate primary ionization and secondary electron ionization, respectively, from precipitating energetic protons in the Earth's upper atmosphere. It is found that secondary electron ionization may be negligible for low-energy proton precipitation ($E_{\text{mono}} \leq 10$ keV), but becomes significant or even comparable to primary proton/hydrogen ionization at higher incident energies, confirming earlier results [e.g., *Lilensten and Galand, 1998*]. The mean energy loss per ion pair production is calculated, which increases nearly monotonically from $W = 22$ eV at $E_{\text{mono}} = 100$ eV to 33 eV at $E_{\text{mono}} = 1$ MeV. It is hard to explain the difference at $E_{\text{mono}} = 1$ MeV with the widely used $W = 35$ eV by range calculation. The small percentage difference of $\sim 6\%$ may either be attributed to oversimplification by range calculation or be due to cross-section incompleteness in our model, or both. In this study, the mean energy loss for Maxwellian proton precipitation is also calculated and in line with the previous results from Monte Carlo models [*Kozelov and Ivanov, 1994; Decker et al., [1996]* and linear transport theoretic models [*Strickland et al., 1993; Galand et al., 1999*], in spite of explainable differences due to model treatments and cross-section selections. It shows that the mean energy loss per ion pair production W provides a valuable way to test the accuracy and completeness of cross-section databases [e.g., *Simon Wedlund et al., 2011*].

[34] As more emphasis is placed on understanding the interplay among Earth's space components from a system viewpoint, a fast and accurate calculation method for ion impact effects is increasingly needed for large-scale computations. To accommodate this need, we have derived a fast calculation method of proton impact total ionization rates in the Earth's upper atmosphere, which is applicable to a wide energy range of monoenergetic particle precipitation from 100 eV to 1 MeV. The advantage of the monoenergetic parameterization is that it is applicable to any incident spectra over a wide range, no matter what form the energy distribution takes. It can be a Maxwellian distribution, a κ distribution, a power law distribution, or of any shape. In order to have ionization results for individual atmospheric species, cross section-based branching ratios may be applied [e.g., *Galand et al., 1999*]. Deriving separate parameterizations for individual ion production rates is subject for future research.

[35] Because the new parameterization is designed for monoenergetic proton precipitation with energy between

100 eV and 1 MeV, caution is needed when applying the decomposition and then integration algorithm described in section 3.3 to an incident spectrum theoretically spanning in energy from 0 to ∞ , such as Maxwellian and κ distributions. In order to have a proper application for these cases, one has to ensure that the energy influx over 100 eV to 1 MeV has a good coverage of the total input. In other words, the ratio as given below should be close to 1.

$$r = \frac{\int_{0.1 \text{ keV}}^{1000 \text{ keV}} E\phi(E)dE}{\int_0^{\infty} E\phi(E)dE}. \quad (9)$$

Selecting $r = 0.99$ (i.e., 1% error in representing the topside particle energy input), our parameterization can be applied to calculate ionization from an incident characteristic energy range of E_0 from 0.23 keV to 119 keV in a Maxwellian distribution (see equation (1)). If the requirement is lessened to $r = 0.95$, the applicable E_0 range becomes 0.122–159 keV. Likewise, for a κ distribution,

$$\phi_{\kappa}(E) = \frac{Q_0}{2E_0^3} \frac{(\kappa-1)(\kappa-2)}{\kappa^2} E \left(1 + \frac{E}{\kappa E_0}\right)^{-\kappa-1}, \quad (10)$$

$\kappa = 5$ corresponds to an applicable E_0 range of 0.169–23.6 keV (for $r = 0.99$) or 0.086–46.7 keV (for $r = 0.95$). Note that the average energy of a κ distribution is $\langle E \rangle = 2\kappa E_0/(\kappa-2)$.

[36] It has been demonstrated that the empirical formulae presented in this paper not only are computational efficient but also generate results as accurate as those directly from the sophisticated coupled model. A systematic error analysis for 50 incident monoenergies and under 36 MSIS-90 atmospheres shows an excellent agreement with the coupled model. The relative errors in the estimates of altitude-integrated ionization and peak ionization are less than $\pm 3\%$ and $\pm 4\%$, respectively. The displacement in the estimated ionization peak altitudes is less than ± 4 km and in most cases less than ± 2 km. This shows that our parameterization, derived from the physics-based model, is robust and can be used for exploring proton impact effects as well as feedbacks in large community models.

[37] **Acknowledgments.** The work was supported by NASA grant NNX09AI04G.

[38] Robert Lysak thanks the reviewers for their assistance in evaluating this paper.

References

- Basu, B., J. R. Jasperse, R. M. Robinson, R. R. Vondrak, and D. S. Evans (1987), Linear transport theory of auroral proton precipitation: A comparison with observations, *J. Geophys. Res.*, **92**, 5920–5932.
- Basu, B., J. R. Jasperse, D. J. Strickland, and R. E. Daniell Jr. (1993), Transport-theoretic model for the electron-proton-hydrogen atom aurora: 1. Theory, *J. Geophys. Res.*, **98**(A12), 21,517–21,532, doi:10.1029/93JA01646.
- Basu, B., D. T. Decker, and J. R. Jasperse (2001), Proton transport model: A review, *J. Geophys. Res.*, **106**(A1), 93–105, doi:10.1029/2000JA002004.
- Berger, M. J., J. S. Coursey, M. A. Zucker, and J. Chang (2011), Stopping-power and range tables for electrons, protons, and helium ions, *NISTIR 4999*, ASTAR Program, NIST Physics Laboratory, <http://www.nist.gov/pml/data/star/index.cfm>.
- Decker, D. T., B. V. Kozelov, B. Basu, J. R. Jasperse, and V. E. Ivanov (1996), Collisional degradation of the proton-H atom fluxes in the atmosphere: A comparison of theoretical techniques, *J. Geophys. Res.*, **101**(A12), 26,947–26,960, doi:10.1029/96JA02679.

- Emery, B. A., V. Coumans, D. S. Evans, G. A. Germany, M. S. Greer, E. Holeman, K. Kadinsky-Cade, R. J. Rich, and W. Xu (2008), Seasonal, Kp, solar wind, and solar flux variations in long-term single-pass satellite estimates of electron and ion auroral hemispheric power, *J. Geophys. Res.*, *113*, A06311, doi:10.1029/2007JA012866.
- Fang, X., M. W. Liemohn, J. U. Kozyra, and S. C. Solomon (2004), Quantification of the spreading effect of auroral proton precipitation, *J. Geophys. Res.*, *109*, A04309, doi:10.1029/2003JA010119.
- Fang, X., M. W. Liemohn, J. U. Kozyra, and S. C. Solomon (2005), Study of the proton arc spreading effect on primary ionization rates, *J. Geophys. Res.*, *110*, A07302, doi:10.1029/2004JA010915.
- Fang, X., M. W. Liemohn, J. U. Kozyra, and D. S. Evans (2007a), Global 30–240 keV proton precipitation in the 17–18 April 2002 geomagnetic storms: 2. Conductances and beam spreading, *J. Geophys. Res.*, *112*, A05302, doi:10.1029/2006JA012113.
- Fang, X., A. J. Ridley, M. W. Liemohn, J. U. Kozyra, and D. S. Evans (2007b), Global 30–240 keV proton precipitation in the 17–18 April 2002 geomagnetic storms: 3. Impact on the ionosphere and thermosphere, *J. Geophys. Res.*, *112*, A07310, doi:10.1029/2006JA012144.
- Fang, X., C. E. Randall, D. Lummerzheim, S. C. Solomon, M. J. Mills, D. R. Marsh, C. H. Jackman, W. Wang, and G. Lu (2008), Electron impact ionization: A new parameterization for 100 eV to 1 MeV electrons, *J. Geophys. Res.*, *113*, A09311, doi:10.1029/2008JA013384.
- Fang, X., C. E. Randall, D. Lummerzheim, W. Wang, G. Lu, S. C. Solomon, and R. A. Frahm (2010), Parameterization of monoenergetic electron impact ionization, *Geophys. Res. Lett.*, *37*, L22106, doi:10.1029/2010GL045406.
- Galand, M., R. G. Roble, and D. Lummerzheim (1999), Ionization by energetic protons in Thermosphere-Ionosphere Electrodynamics General Circulation Model, *J. Geophys. Res.*, *104*, 27,973–27,989.
- Galand, M., T. J. Fuller-Rowell, and M. V. Codrescu (2001), Response of the upper atmosphere to auroral protons, *J. Geophys. Res.*, *106*(A1), 127–139.
- Galand, M., and A. D. Richmond (2001), Ionospheric electrical conductances produced by auroral proton precipitation, *J. Geophys. Res.*, *106*(A1), 117–125, doi:10.1029/1999JA002001.
- Guo, J., X. Feng, B. A. Emery, J. Zhang, C. Xiang, F. Shen, and W. Song (2011), Energy transfer during intense geomagnetic storms driven by interplanetary coronal mass ejections and their sheath regions, *J. Geophys. Res.*, *116*, A05106, doi:10.1029/2011JA016490.
- Hardy, D. A., M. S. Gussenhoven, and D. Brautigam (1989), A statistical model of auroral ion precipitation, *J. Geophys. Res.*, *94*, 370–392.
- Hedin, A. E. (1991), Extension of the MSIS Thermosphere Model into the middle and lower atmosphere, *J. Geophys. Res.*, *96*, 1159–1172.
- Jackman, C. H., J. E. Frederick, and R. S. Stolarski (1980), Production of odd nitrogen in the stratosphere and mesosphere: An intercomparison of source strengths, *J. Geophys. Res.*, *85*(C12), 7495–7505.
- Jasperse, J. R., and B. Basu (1982), Transport theoretic solutions for auroral proton and H atom fluxes and related quantities, *J. Geophys. Res.*, *87*, 811–822.
- Kallio, E., and S. Barabash (2001), Atmospheric effects of precipitating energetic hydrogen atoms on the Martian atmosphere, *J. Geophys. Res.*, *106*, 165–177.
- Kozelov, B. V. (1993), Influence of the dipolar magnetic field on transport of proton-H atom fluxes in the atmosphere, *Ann. Geophys.*, *11*, 697–704.
- Kozelov, B. V., and V. E. Ivanov (1994), Effective energy loss per electron-ion pair in proton aurora, *Ann. Geophys.*, *12*, 1071–1075.
- Lanchester, B., O.-P. Jokiahio, M. Galand, N. Ivchenko, D. Lummerzheim, J. Baumgardner, and S. Chakrabarti (2011), Separating and quantifying ionospheric responses to proton and electron precipitation over Svalbard, *J. Geophys. Res.*, *116*, A09322, doi:10.1029/2011JA016474.
- Lilensten, J., and M. Galand (1998), Proton-electron precipitation effects on the electron production and density above EISCAT (Tromsø) and ESR, *Ann. Geophys.*, *16*, 1299–1307.
- Lummerzheim, D., M. H. Rees, and H. R. Anderson (1989), Angular dependent transport of auroral electrons in the upper atmosphere, *Planet. Space Sci.*, *37*, 109–129.
- Lummerzheim, D., and J. Lilensten (1994), Electron transport and energy degradation in the ionosphere: Evaluation of the numerical solution, comparison with laboratory experiments and auroral observations, *Ann. Geophys.*, *12*, 1039–1051.
- Lyons, L. R., and D. S. Evans (1984), An association between discrete aurora and energetic particle boundaries, *J. Geophys. Res.*, *89*, 2395–2400.
- McNeal, R. J., and J. H. Birely (1973), Laboratory studies of collisions of energetic H⁺ and hydrogen with atmospheric constituents, *Rev. Geophys.*, *11*, 633–692.
- Rees, M. H. (1982), On the interaction of auroral protons with the Earth's atmosphere, *Planet. Space Sci.*, *30*, 463–472.
- Sharber, J. R. (1981), The continuous (diffuse) aurora and auroral-E ionization, in *Physics of Space Plasma*, vol. 7, edited by T. S. Chang, B. Coppi, and J. R. Jasperse, 115 pp., Scientific, Gainesville, Fla.
- Simon Wedlund, C., G. Gronoff, J. Lilensten, H. Ménager, and M. Barthélemy (2011), Comprehensive calculation of the energy per ion pair or *W* values for five major planetary upper atmospheres, *Ann. Geophys.*, *29*(1), 187–195, doi:10.5194/angeo-29-187-2011.
- Solomon, S. C. (2001), Auroral particle transport using Monte Carlo and hybrid methods, *J. Geophys. Res.*, *106*, 107–116.
- Strickland, D. J., R. E. Daniell Jr., J. R. Jasperse, and B. Basu (1993), Transport-theoretic model for the electron-proton-hydrogen atom aurora: 2. Model results, *J. Geophys. Res.*, *98*(A12), 21,533–21,548, doi:10.1029/93JA01645.